Chapter 2

Experimental

In this dissertation, mainly characterizations on structural and optical properties of RE doped GaN were carried out. Various characterization tools are hired to examine various sample properties. In this chapter, short explanations of the experimental skills and concepts of each characterization will be described.

2.1 Sample growth using gas source molecular beam epitaxy (GSMBE)

Sample growth was performed by adopting a gas source molecular beam epitaxy (GSMBE) using ammonia (NH_3) gas for nitrogen (N)source. Fig. 2-1 shows the schematic diagram of Eiko ammonia gas source MBE system used in this study. All substrates, unless otherwise noted, used in this dissertation were sapphire (Al_2O_3)(0001). For usual Al_2O_3 (0001) substrate, conventional pre-treatment was preceded. Ultrasonic surface cleaning using organic solvents such as acetone (CH_3COCH_3) and methyl alcohol (CH_3OH) was carried out. And then surface etching (flattening) of the substrates were performed by dipping in 120°C heated sulfuric acid (H_2SO_4) and phosphoric acid (H_3PO_4) mixed (3:1 molar fraction) solution for 20 minutes to remove scratches on the surface which came from mechanical polishing. E-beam molybdenum (Mo) coating was carried out on the back side of substrate (the other side of the growth surface) to avoid forming thermal islands. The substrate was glued on Mo block by melted indium (In) and held by thin Mo pin to avoid dropping at high growth temperatures. The substrate on Mo block was then introduced in preparation chamber, and transferred into growth chamber without breaking the vacuum. The background vacuum of growth chamber reached was 1×10^{-10}torr. The atmospheric components in the growth chamber were monitored by quadrupole mass spectrograph (QMS). The surface morphology of the sample was *in situ* observed by Reflection High Energy Electron Diffraction (RHEED). Metallic gallium (Ga) with 6-nine purity and RE with 3-nine purity was evaporated from conventional Knudsen effusion cells. Uncracked NH_3 gas with 6-nine purity was used for nitrogen source. The NH_3 was introduced into growth chamber through a nozzle of stainless-steel tube, and the pressure was controlled by valuable leak valve.

Fig. 2-2 shows the typical growth sequence of RE doped GaN. Prior to the main growth, the surface of sapphire substrate was thermally cleaned and nitridation was carried out under 4×10^{-4}torr of ammonia pressure for 20 minutes at substrate temperature over 900°C. Then the substrate was cooled down to lower than 600°C for the growth of 20 nm-thick "low temperature" GaN buffer layer at Ga cell temperature of 950°C and NH_3 pressure of 3×10^{-5}torr. Next, the substrate temperature was heated up to 950°C and maintained for 5 minutes for annealing. Then the substrate temperature was set to the growth temperature of main growth. For the main growth, the substrate temperature, Ga cell temperature, NH_3 pressure was varied on the range of 550~900°C, 870~980°C, and 1×10^{-6}~3×10^{-5}torr, respectively, for each growth conditions and RE doping was initiated simultaneously -or after some amount of undoped GaN growth was preceded.

2.2 Characterization

2.2.1 Reflection High Energy Electron Diffraction (RHEED)

RHEED is an established technique which is widely used as an *in situ* probe to monitor the growth of thin films both in research and in industry[2-1, 2, 3, 4, 5, 6]. Fig. 2-3 shows a schematic diagram of

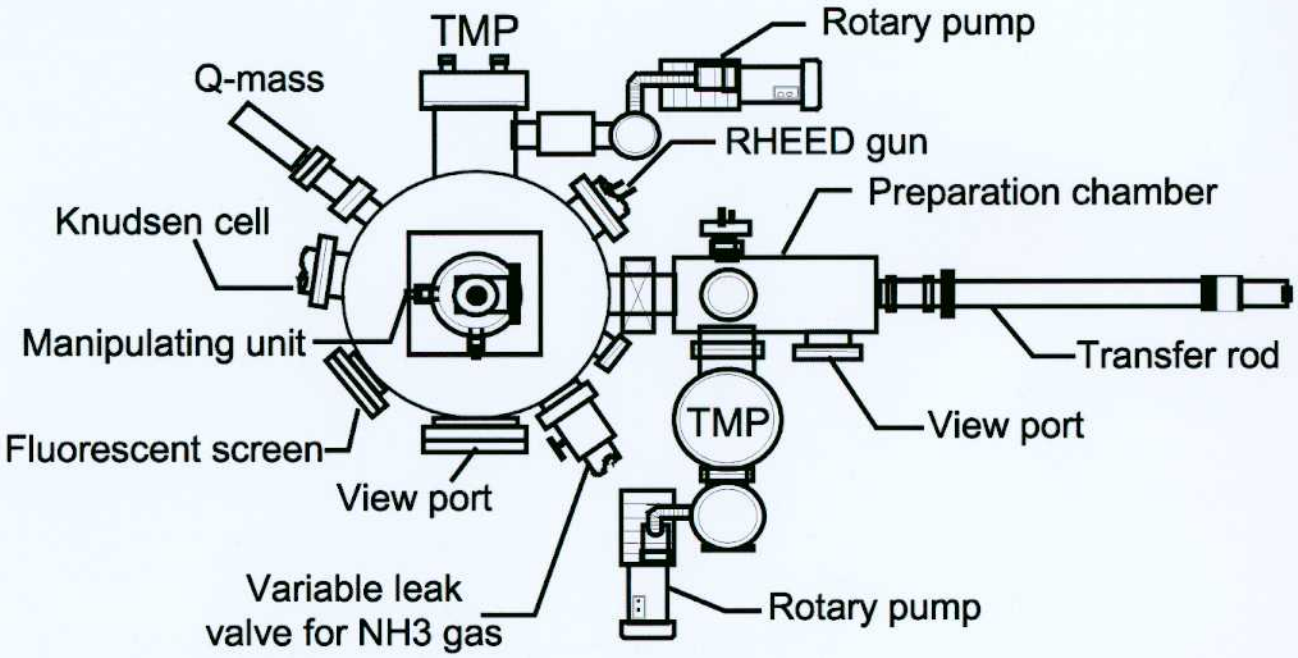

Figure 2-1: Schematic diagram of EIKO-Ammonia-MBE system

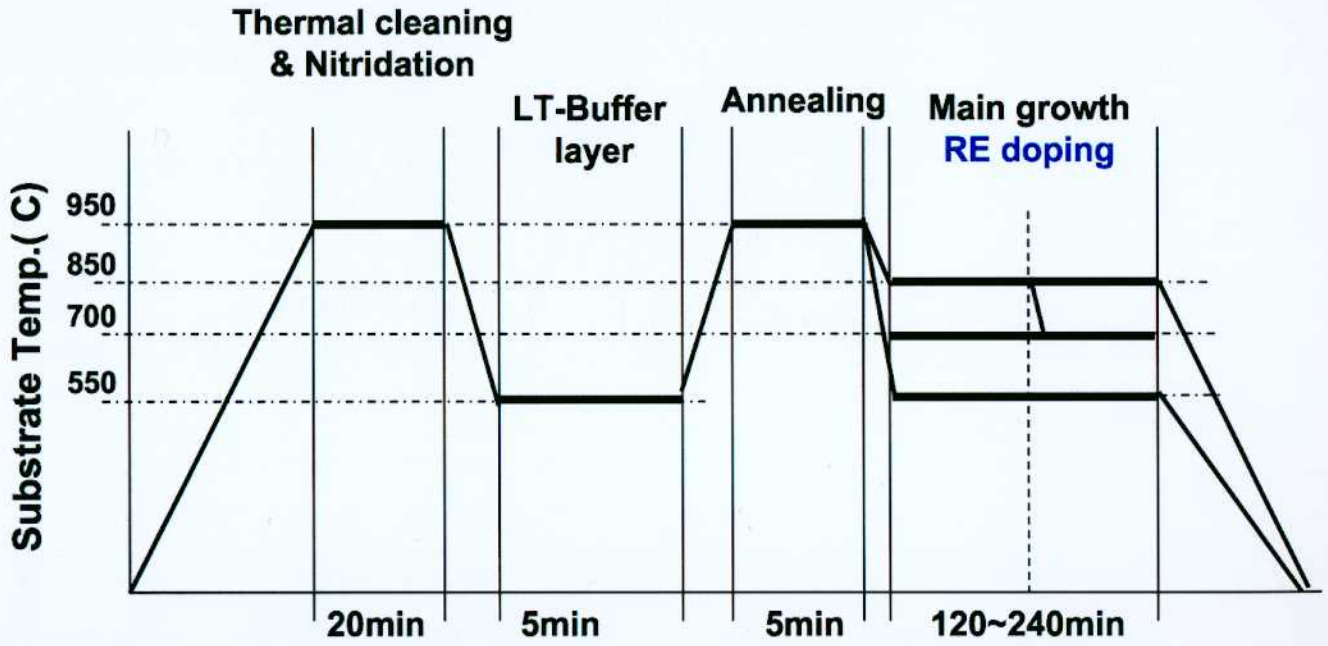

Figure 2-2: The typical growth sequence of RE doped GaN

RHEED apparatus. An electron beam with high energy (5~100keV) is directed at the sample surface at a glancing angle (<~3°). The high energy of the electrons would result in high penetration depth. However, because of the glancing angle of incidence, a few atomic layers are only probed. This is the reason of the high surface sensitivity of RHEED. The result of electron diffraction, diffraction pattern, which depends on the surface morphology and structure, forms on phosphor screen mounted opposite to the electron gun.

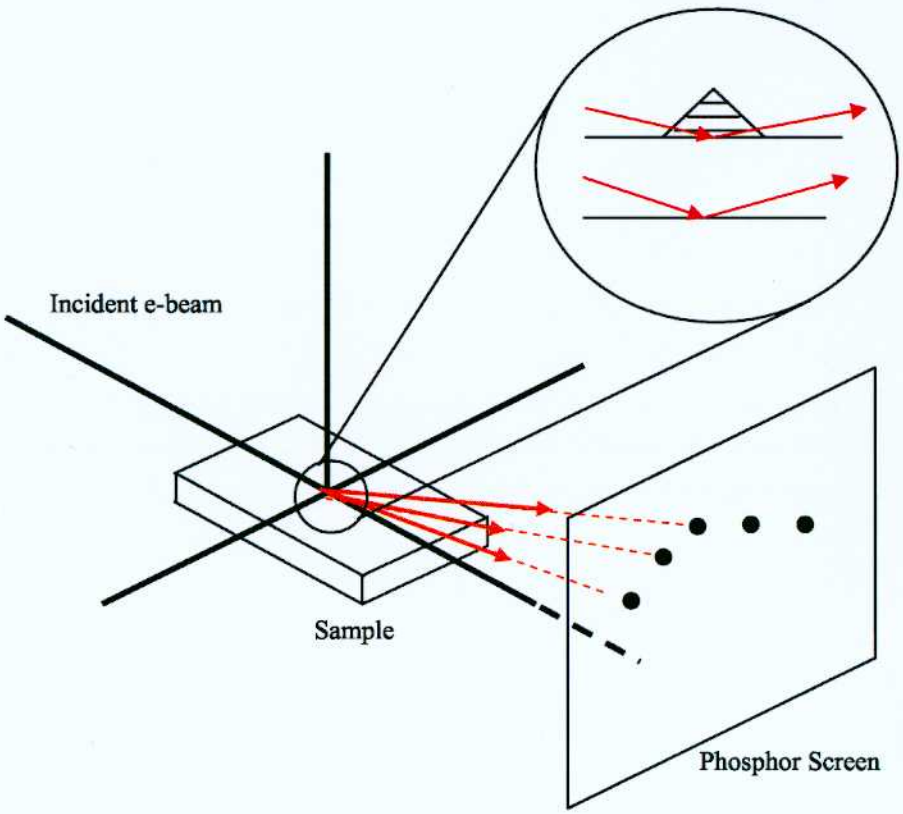

Figure 2-3: An illustration of the fundamentals of RHEED [2-8]. The inset shows two kinds of reflections: transmission-reflection diffraction scattering by three-dimensional crystalline island (above) and surface scattering from flat surface (below).

An example of the RHEED surface sensitivity is shown in Fig. 2-4, in which a comparison between RHEED patterns obtained for reconstructed and non-reconstructed surfaces, is given. Conceptually, perfectly flat surfaces should result in a diffraction pattern that consists of spots arranged on Laue rings, Fig. 2-4 (b). However, because of the non-idealities in the electron beam and the sample's surface, streaks appear instead of spots as shown in Fig. 2-4 (a). From the spacing between streaks, the lattice spacing can be estimated, and the oscillation on reflection intensity of pattern, the growth step of every mono layer can be directly measured and this makes the dexterous control of quantum structure possible.

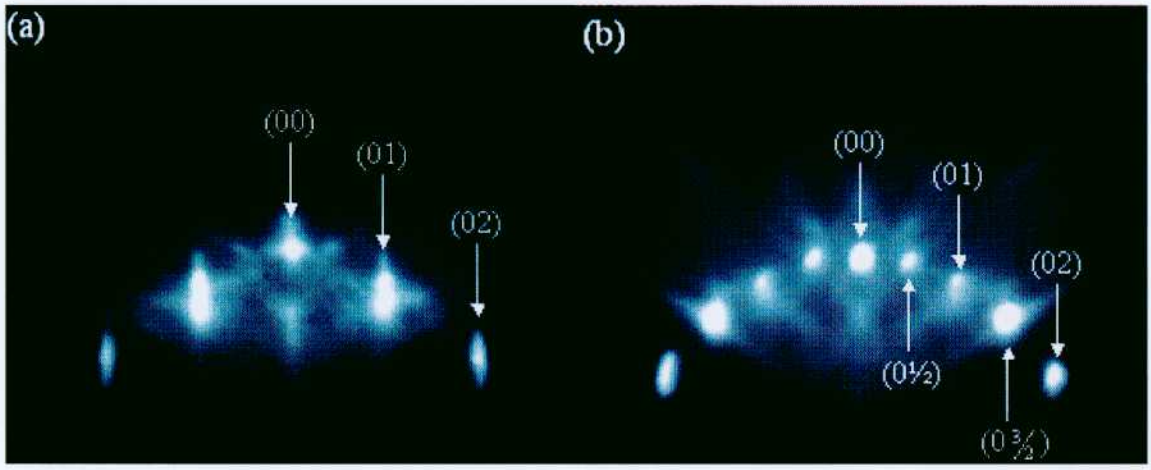

Figure 2-4: RHEED is sensitive for surface structures and reconstructions. (a) Si(100)-1x1 obtained by chemically cleaning the sample and loading it to the vacuum within few minutes [electron beam is incident in the ⟨110⟩ with 8.6 keV], (b) Si(100)-2×1 reconstructed surface, obtained by chemically-cleaning the sample then baking the system for two days and flashing it up to 1200°C [electron beam is incident in the ⟨110⟩ with 8.6 keV][2-8].

Most surfaces are not perfectly flat; hence, the diffraction pattern is produced by transmission through the surface roughness (asperities); see the inset of Fig. 2-3. Despite the popularity of RHEED, there is no complete formal theory for it. However, a number of simplified kinematical approaches have been introduced that are useful for understanding the basic idea of RHEED. They are sufficient for the determination of the unit cell dimension, crystal orientation and the crystal shape. The lack of a formal theory is the reason behind the debate over the interpretation of RHEED results [2-7].

2.2.2 Atomic Force Microscopy (AFM)

To evaluate surface morphology of RE and undoped GaN, various microscopy were hired. AFM is one of the equipment for micrographic studies [2-9]. The principles on how the AFM works are very simple. The conceptual setup of AFM is shown in Fig. 2-5.

An atomically sharp tip is scanned over a surface with feedback mechanisms that enable the piezo-electric scanners to maintain the tip at a constant force (to obtain height information), or height (to obtain force information) above the sample surface. Tips are typically made from Si_3N_4 or Si, and extended down from the end of a cantilever. The nanoscope AFM head employs an optical detection system in which the tip is attached to the underside of a reflective cantilever. A diode laser is focused onto the back of a reflective cantilever. As the tip scans the surface of the sample, moving up and down with the contour of the surface, the laser beam is deflected off the attached cantilever into a dual element photodiode. The photodetector measures the difference in light intensities between the upper and lower photodetectors, and then converts to voltage. Feedback from the photodiode

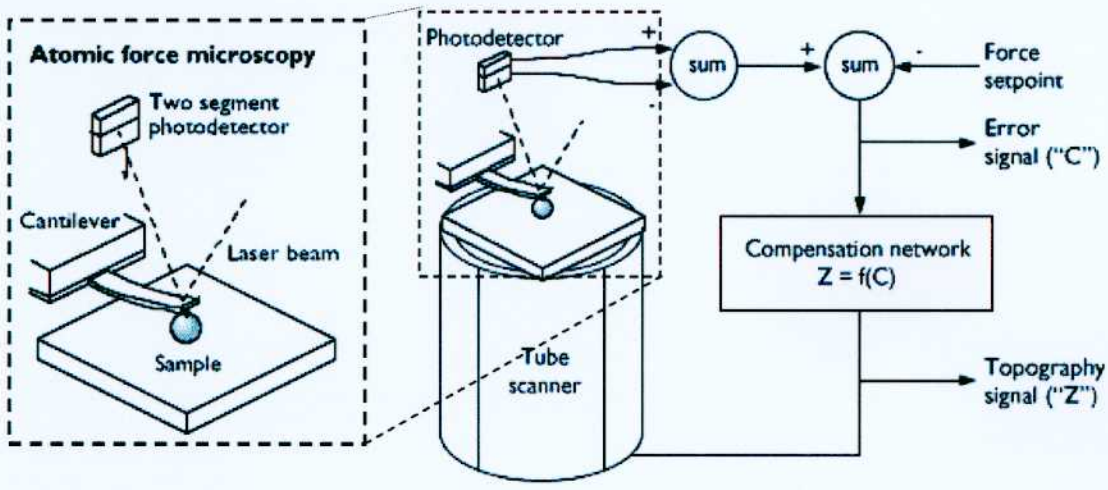

Figure 2-5: The AFM feedback loop. A compensation network monitors the cantilever deflection and keeps it constant by adjusting the height of the sample (or cantilever)[2-10].

difference signal, through software control from the computer, enables the tip to maintain either a constant force or constant height above the sample. In the constant force mode the piezo-electric transducer monitors real time height deviation. In the constant height mode the deflection force on the sample is recorded. The latter mode of operation requires calibration parameters of the scanning tip to be inserted in the sensitivity of the AFM head during force calibration of the microscope. Some AFM's can accept full 200 mm wafers. The primary purpose of these instruments is to quantitatively measure surface roughness with a nominal 5 nm lateral and 0.01nm vertical resolution on all types of samples. Depending on the AFM design, scanners are used to translate either the sample under the cantilever or the cantilever over the sample. By scanning in either way, the local height of the sample is measured. Three dimensional topographical maps of the surface are then constructed by plotting the local sample height versus horizontal probe tip position.

2.2.3 Transmission electron microscope (TEM)

Materials for TEM must be specially prepared for various levels of thickness, which allow electrons to transmit through the sample, much like light is transmitted through materials in conventional optical microscopy. Because the wavelength of electrons is much smaller than that of light, the optimal resolution attainable for TEM images is many orders of magnitude better than that from a light microscope. Thus, TEMs can reveal the finest details of internal structure - in some cases as small as individual atoms. Magnifications of 350,000 times can be routinely obtained for many materials, whilst in special circumstances, atoms can be imaged at magnifications greater than 15 million times. The energy of the electrons in the TEM determines the relative degree of penetration of electrons in a specific sample, or alternatively, influence the thickness of material from which useful information

may be obtained. Because of the high spatial resolution obtained, TEMs are often employed to determine the detailed crystallography of fine-grained, or rare, materials. Thus, for the physical and biological sciences, TEM is a complementary tool to conventional crystallographic methods such as X-ray diffraction[2-11].

2.2.4 Scanning Electron Microscope (SEM)

SEM is one of the most versatile and widely used tools of modern science as it allows the study of both morphology and composition of biological and physical materials. In this study, the morphology of sample surface of RE doped GaN was observed by SEM, and compared with the results of AFM. In SEM, an electron beam is focused into a small probe and is rastered across the surface of a specimen. Several interactions with the sample that result in the emission of electrons or photons occur as the electrons penetrate the surface. These emitted particles can be collected with the appropriate detector to yield valuable information about the material. The schematic diagram of SEM is shown in Fig. 2-6.

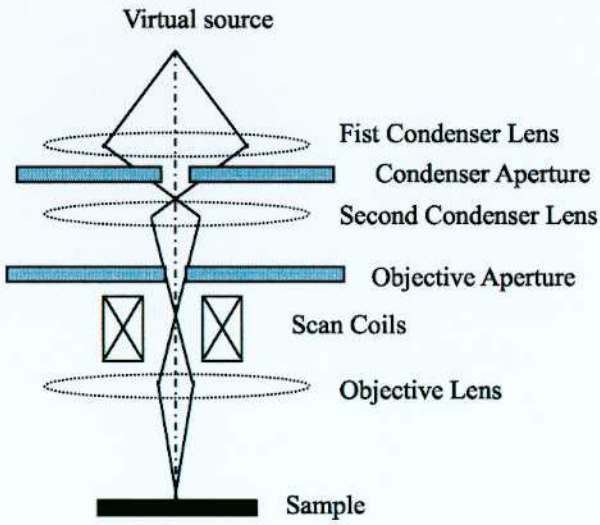

Figure 2-6: Schematic diagram of SEM

2.2.5 X-ray diffraction (XRD)

XRD is one of the most fundamental and widely-used characterization tools among which use X-ray radiation [2-12, 13]. The information about the lattice constant, azimuth, stability of crystal arrangement can be obtained. The typical XRD diffractometer for theta-2theta method are shown in Fig. 2-7 (a). The diffractometter consists of X-ray generation part, goniometer and detecter. There are many ways to generate X-rays, but for this study, X-ray was produced by electron collision into

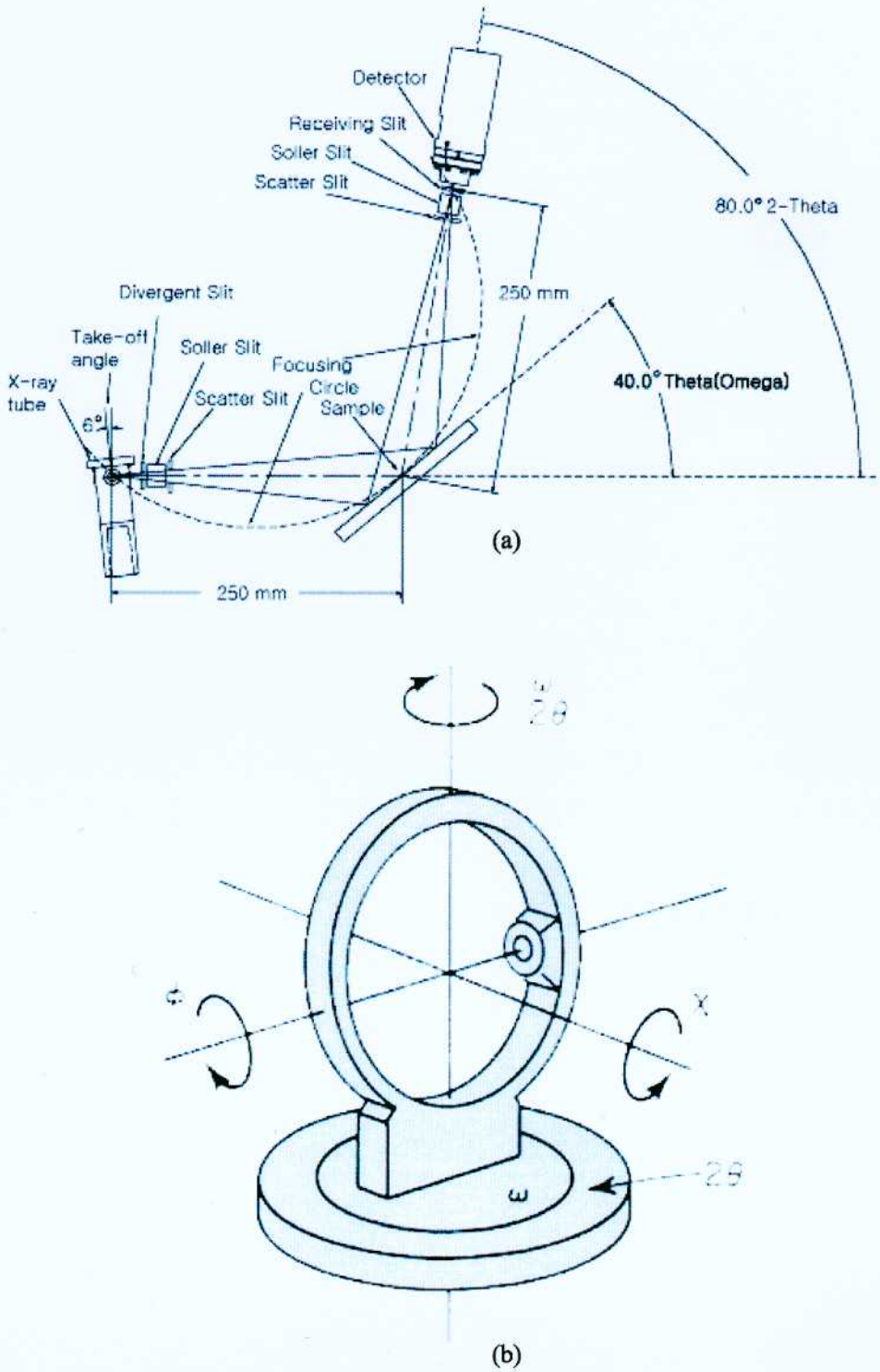

Figure 2-7: (a) Typical theta(ω)-2theta XRD setup and (b) 4 axis goniometer.[2-14]

Cu target in filament tube. Thorough the crystal spectrometer (monochrometer), specific wavelengths (Cu-$K_{\alpha 1}$:1.5406Å, $K_{\alpha 2}$:1.5444Å) of X-rays are irradiated into sample crystal. In 2 axis diffractometer, the rotation angle of sample holder and X-ray has ratio of 1:2. The relation between the X-ray wavelength and the diffraction beam angle is defined as Bragg's raw,

$$2dsin\theta = \lambda$$

Where λ is incident X-ray wavelength, d is the length of lattice spacing and θ is the diffraction angle. Therefore, at a specific angle 2θ the relevant intensity of X-ray wavelength can be obtained. This is why this method is called the theta(ω)-2theta mode. In theta(ω) -2theta mode, variations of lattice plane spacings are detected, and the observed peak width corresponds to the width of each reciprocal lattice point parallel to the diffraction vector. For epitaxial layer used in this study, only the plane spacings parallel to the film surface are usually measured. In order to characterize inclines caused by tilts and twists, off axis plane which is hard to be examined in theta(ω)-2theta mode, a 4 axis goniometer as shown in Fig. 2-7 (b) was used for ω scan and reciprocal lattice mapping.

2.2.6 Rutherford back-scattering (RBS)

RBS [2-15] is an analytical tool that uses elastic scattering of 0.1-3 MeV charged particles to analyze the surface and the outer few micrometers of solids. A typical RBS system consists of an accelerator and scattering chamber with sample manipulators and particle detectors. In this study, RBS measurements were performed at room temperature with 2 MeV He ion beam at The Institute of Physical and Chemical Research (RIKEN). The He ion beam was collimated to give divergence less than 0.076° . The beam current and size were about 1.5 nA and 1mm in diameter, respectively. The backscattered He ions were measured with a surface-barrier Si detector placed at an angle of 160° with respect to the incident beam. The sample was mounted on a three-axes goniometer and channeling angular profiles were obtained for the ⟨0001⟩ channel. Theoretical explanations are followed.

As illustrated in the Fig. 2-8, an ion with mass M_1 is accelerated with energy E_0 and then irradiated to a solid consisting of an atom with mass M_2. The ion is ricochet off the surface of the atom as elastic scattering. The energy E_1 of this ion is shown by the following equation:

$$E_1 = K_{in} \cdot E_0$$

$$K_{in} = \left[\frac{M_1 cos\theta + \sqrt{M_2^2 - M_1^2 sin^2\theta_s}}{M_1 + M_2} \right]^2$$

where K_{in} stands for Kinematical Factor. According to the above equation, the energy of the incident ion recoiled as elastic scattering is expressed as a function of the mass M_2 of the atomic nucleus. This means that the mass of the corresponding element can be estimated from the energy spectrum of the

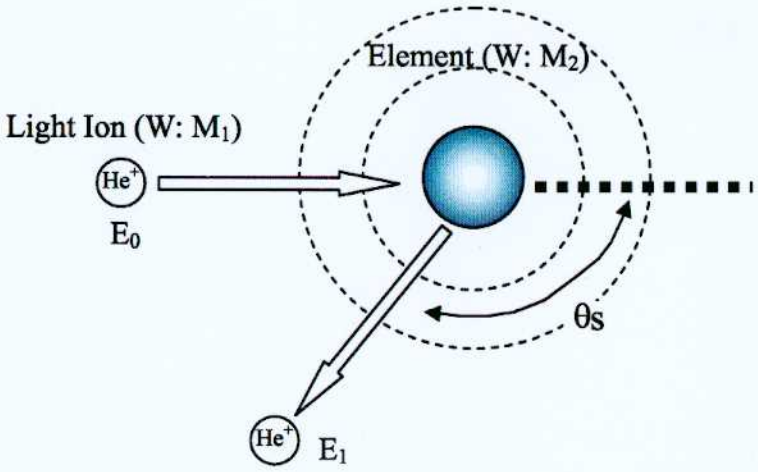

Figure 2-8: Rutherford Back scattering

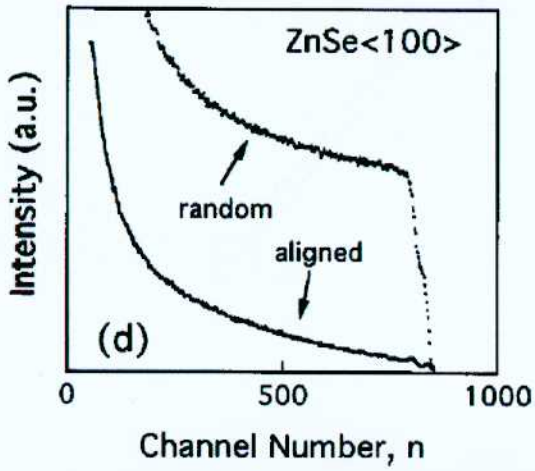

Figure 2-9: RBS random and ⟨100⟩ aligned spectra of ZnSe [2-16]

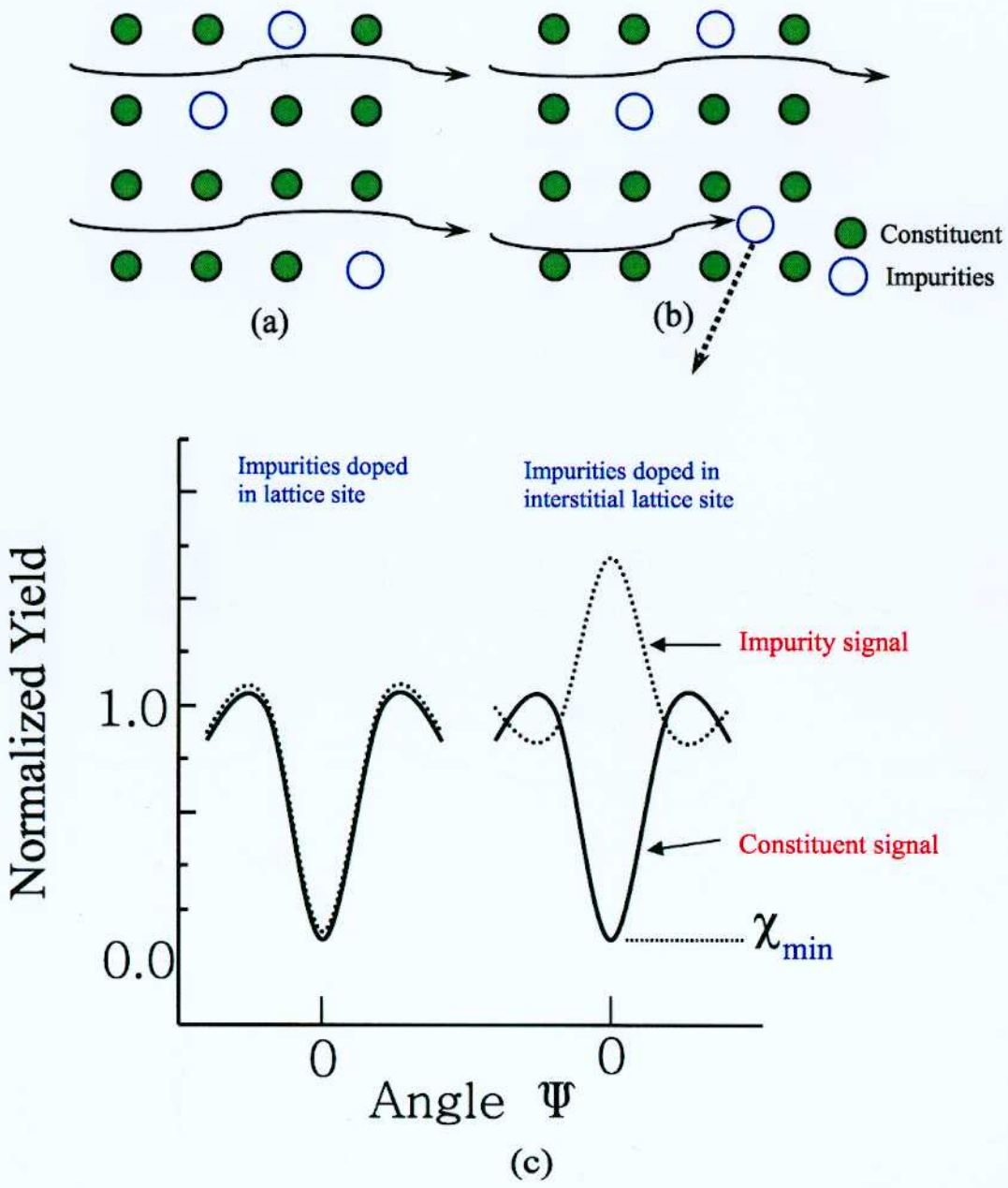

Figure 2-10: The concept of RBS ion channeling. When impurities are doped in (a)lattice sites and (b) interstitial sites. (c) The incident beam angular dependency on backscattering yield is also shown.

scattered ions. Especially when the back-scattered ions (θ_s=180°) are used, the resolution becomes highest. This is used as RBS. On the other hand, the ions that have been scattered atΔX from the sample surface lose their energy due to knock-on scattering (inelastic scattering) with orbital electrons in the solid at their incoming/outgoing time. Thus, the energy of the scattered ions becomes lower byΔE than E_1. In the solid, ΔE is almost linearly in proportion to ΔX. From this ΔE, the depth ΔX of the atomic nucleus with which the ion has collided can be found. A spectrum, for example, for film extends like a band and this width corresponds to the thickness of the film. Therefore, even multi-layered film can be measured to obtain the thickness of each of all the layers by a single irradiation. This capability of non destructively measuring elemental distribution in the depth direction provides incomparably higher reliability and throughput compared to the conventional analysis methods.

2.2.7 RBS/ ion channeling

If the sample is crystal, a more interesting phenomenon will occur. Normally the incident ions collide with atoms mid-way and are scattered. However, if ions enter the sample in parallel with the crystal axis, they will meander through space among crystal atoms. This phenomenon is called channeling. At this time, the number of backscattered ions decreases markedly. Fig. 2-9 shows the difference between the spectrum obtained in the normal case and that obtained in the channeling case. If crystallinity is low, or when impurities are doped into the interstitial site, there are a number of atoms deviating from the crystal lattice. Accordingly, the number of scattered ions increases and the resulting spectrum increasingly looks like the one obtained when ions are implanted in a direction deviating from the crystal axis. The concept can be understood by Fig. 2-10. The use of this phenomenon allows you to quantitatively evaluate crystallinity and locate atoms between lattices.

2.2.8 Extended X-ray absorption fine structure (EXAFS)

To study the local structure around RE ions, EXAFS[2-17]analysis was carried out on L_{III} edge of RE ions.

A monochromatic X-ray beam is directed at the sample. The photon energy of the X-rays is gradually increased such that it traverses one of the absorption edges of the elements contained within the sample. Below the absorption edge, the photons cannot excite the electrons of the relevant atomic level and thus absorption is low. However, when the photon energy is just sufficient to excite the electrons, then a large increase in absorption occurs known as the absorption edge. (Fig. 2-11(a)) shows absorption spectrum of Ga K-edge InGaN for example). The resulting photoelectrons have a low kinetic energy and can be backscattered by the atoms surrounding the emitting atom (Fig. 2-11(b)). The probability of backscattering is dependent on the energy of the photoelectrons. The backscattering of the photoelectron affects whether the X-ray photon is absorbed in the first place. Hence, the probability of X-ray absorption will depend on the photon energy (as the photoelectron

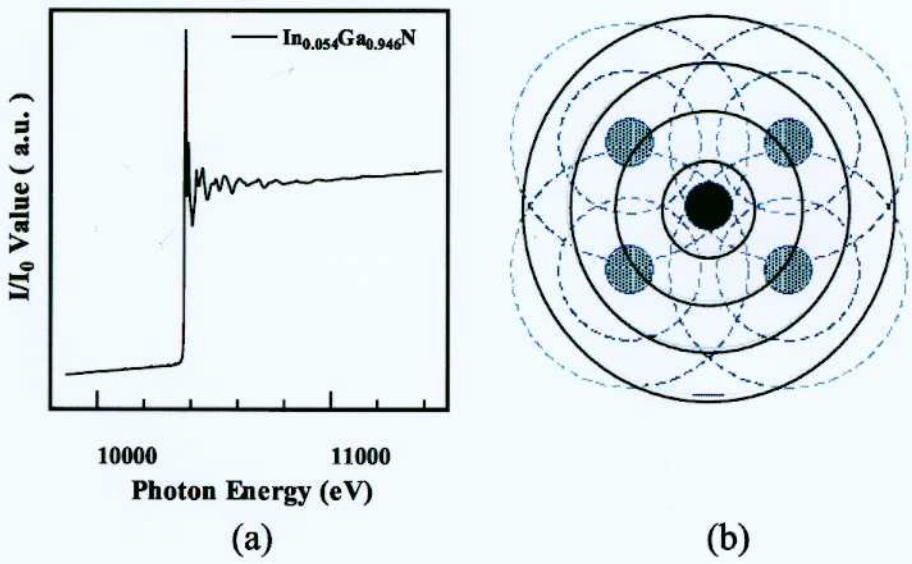

Figure 2-11: (a) Ga K-edge X-ray absorption spectrum of $In_{0.054}Ga_{0.946}N$ at RT[2-21].(b) A schematic diagram of the radial portion of the photoelectron wave (solid lines) being backscattered by the neighboring atoms (dotted lines)

energy will depend on the photon energy). The net result is a series of oscillations on the high photon energy side of the absorption edge. These oscillations can be used to determine the atomic number, distance and coordination number of the atoms surrounding the element whose absorption edge is being examined. The necessity to sweep the photon energy implies the use of synchrotron radiation in EXAFS experiments. The measurement of EXAFS absorption spectra was carried out on beamline(BL)-12C at Photon Factory in High Acceleration Research Organization (KEK, Tsukuba, Japan). The procedures of EXAFS analysis are as follow. From the obtained raw data, background subtraction was carried out and normalized by μ_0 (the smoothly varying portion of μ past the edge and physically corresponds to the absorption coefficient of the free atom) then EXAFS function $\chi(k)$ was extracted (Eq. 2-1).

$$\chi(k) = (\mu - \mu_0)/\mu_0 \qquad \text{(Eq. 2-1)}$$

EXAFS is conveniently described in k space, where k is the photoelectron wave-vector related to the photon energy, E, by

$$k = \left\{2m_e(E - E_0)/\hbar^2\right\}^{1/2} \qquad \text{(Eq. 2-2)}$$

where E_0 is the threshold energy of the absorption edge and m_e is the mass of the electron By performing Fourier transform (FT) (Eq. 2-2), the EXFAS function expressed in momentum space

transformed into radial distribution function (RDF) in R space.

$$\Phi(R) = \frac{1}{\sqrt{2\pi}} \int_{k_{min}}^{k_{max}} \omega(k) k^n \chi(k) \cdot exp(-2ikR) dk \qquad \text{(Eq. 2-3)}$$

Here, $\omega(k)$ is a window-function to diminish the cut-off effect which causes high frequency noise in R space. Weighting scheme (k^n) was applied in order to compensate for the attenuation of the EXAFS amplitude at high k values. This results in clearer resolution of two closely located peaks in Fourier transforms. For a substance constitute by one element, correct RDF can be derived by FT when phase function is taken into account. However, for a substance which is constituted by more than 2 elements, the FT does not include phase function so the resulting RDF shows 0.2 0.5 Å shrunken interatomic distances than the actual one. Fourier filtering technique was applied in RDF to perform curve fitting (Eq.2-4).

$$k^n \chi(k) = \frac{1}{\sqrt{2\pi}} \int_{R_{min}}^{R_{max}} \omega(R) \Phi(R) \cdot exp(-2ikR) dR \qquad \text{(Eq. 2-4)}$$

To get correct RDF, various curve fitting methods do exist. One of representative method is using standard sample of which the structure are already known. To comparing the signal from substance to that from standard sample, one can derive correct curve fit[2-18, 19]. One of the other methods is using theoretical model. In this study the theoretical curve was calculated using FEFF8 [2-20] software to perform curve fitting. The bond length, coordination number, and Debye-Waller factor were used as fitting parameters to yield optimum values.

2.2.9 Photoluminescence (PL) Spectroscopy

PL spectroscopy is a contactless, nondestructive method of probing the electronic structure of materials. Specifically, light is directed onto a sample, where it is absorbed and imparts excess energy into the material in a process called "photo-excitation." One way this excess energy can be dissipated by the sample is through the emission of light, or luminescence. In the case of photo-excitation, this luminescence is called photoluminescence. The intensity and spectral content of this PL is a direct measure of various important material properties. More specifically, photo-excitation causes electrons within the material to move into permissible excited states. When these electrons return to their equilibrium states, the excess energy is released and may include the emission of light (a radiative process) or may not (a nonradiative process). The energy of the emitted light related to the difference in energy levels between the two electron states involved in the transition between the excited state and the equilibrium state. The possible emission processses in PL are shown in Fig. 2-12. The quantity of the emitted light is related to the relative contribution of the radiative process. Through the PL spectroscopy, following analysis can be done.

a. Band gap determination: The most common radiative transition in semiconductors is between states in the conduction and valence bands, with the energy difference being known as the band gap. Band gap determination is particularly useful when working with new compound semiconductors.

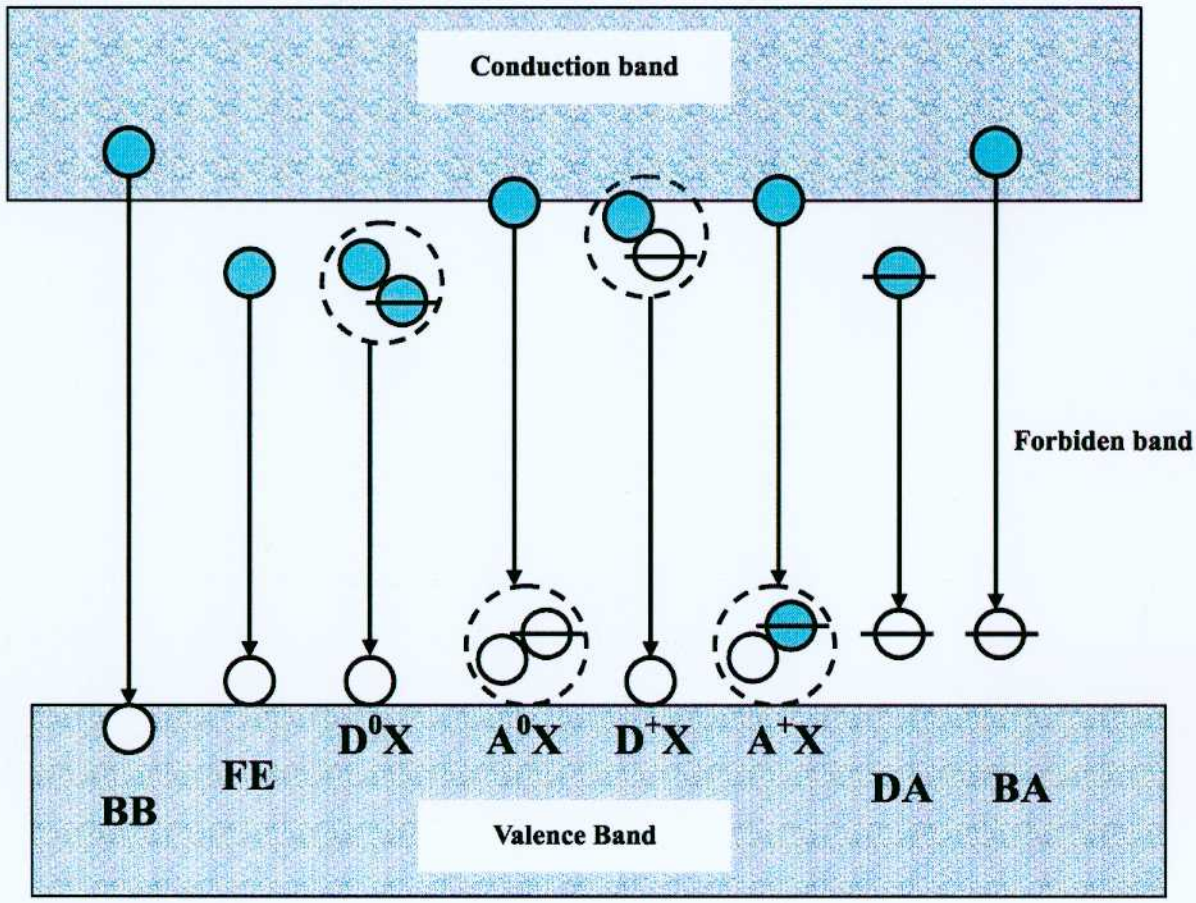

BB : Band to band

FE : Free Exciton recombination

D^0X : Neutral donor bound exciton recombination

A^0X : Neutral acceptor bound exciton recombination

D^+X : Ionized donor bound exiton recombination

A^+X : Ionized acceptor bound exiton recombination

DA : Donor to acceptor recombination

BA : Band to acceptor recombination

Figure 2-12: Various emission processes in semiconductors.

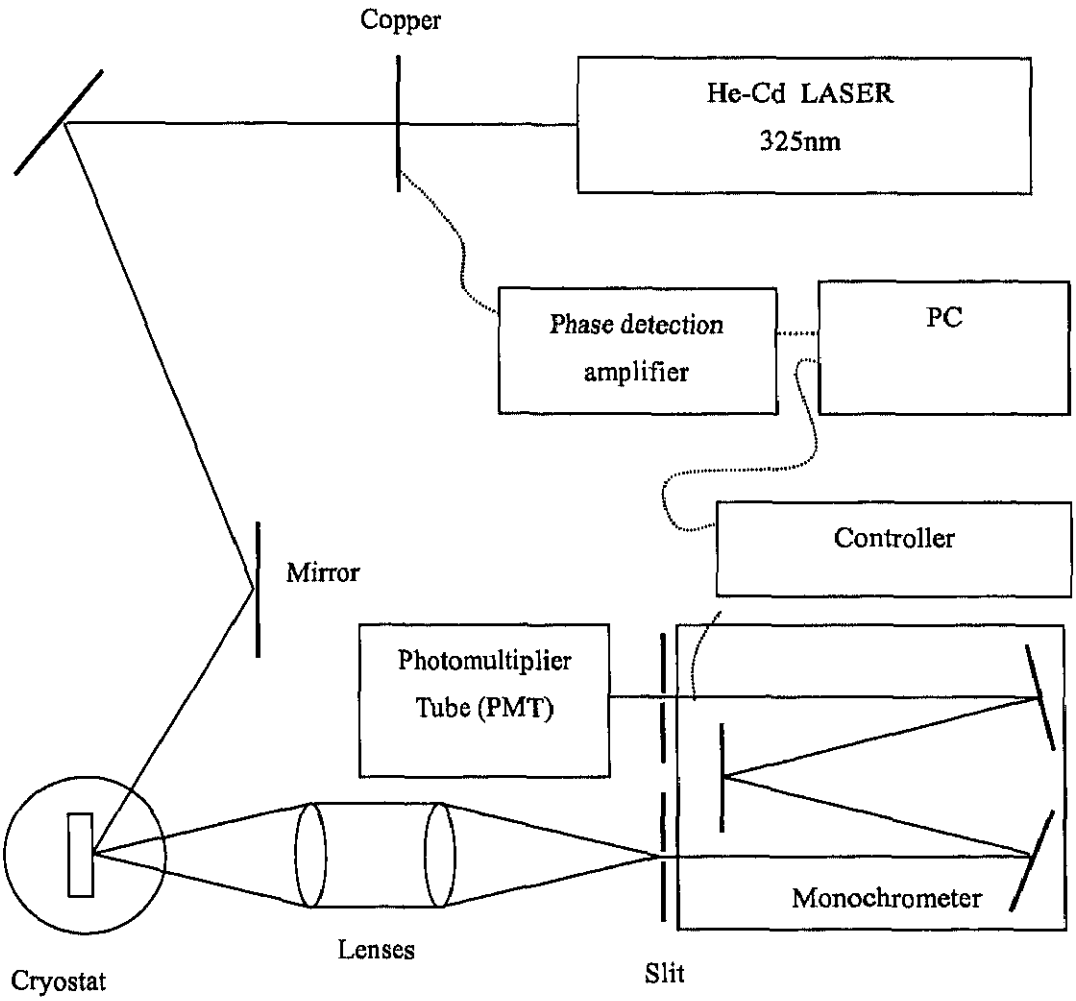

Figure 2-13: Schematic diagram of experimental set up for PL spectroscopy.

b. Impurity levels and defect detection: Radiative transitions in semiconductors also involve localized defect levels. The photoluminescence energy associated with these levels can be used to identify specific defects, and the amount of photoluminescence can be used to determine their concentration.

c. Recombination mechanisms: As discussed above, the return to equilibrium, also known as "recombination," can involve both radiative and nonradiative processes. The amount of photoluminescence and its dependence on the level of photo-excitation and temperature are directly related to the dominant recombination process. Analysis of photoluminescence helps to understand the underlying physics of the recombination mechanism.

d. Material quality: In general, nonradiative processes are associated with localized defect levels, whose presence is detrimental to material quality and subsequent device performance. Thus, material quality can be measured by quantifying the amount of radiative recombination, and etc. Schematic diagram of experimental set up for PL spectro scopy are shown in Fig. 2-13.

2.2.10 Photoluminescence Excitation (PLE)

PLE experiment is the widely used experimental method for the characterization of the sample. Experimental set-up of this experiment is very similar with that of the PL. The difference is that in the PLE experiment, the excitation wavelength rather than the detection wavelength is scanned. For the PLE experiment, wavelength tunable Xe lamp was used as an excitation light source.

2.2.11 Fourier transform infrared spectroscopy (FT-IR)

The absorption of specific wavelengths of infrared radiation is characteristic of chemical bonds, especially the bonds in organic compounds. Thus, the measurement of the infrared absorption spectra is a major tool in the characterization and identification of organic compounds. But in this study, FT-IR spectroscopy was used for the experiment on detection of defect level through the absorption spectra that may relate with electron excitation from defect level which is supposed to relate with energy transfer in RE doped GaN. In modern instruments, the absorption spectrum is measured indirectly, using a Michelson interferometer to record the interference figure produced by combining the radiation transmitted by a sample to radiation transmitted along a variable path within the interferometer. A mathematical function, the Fourier transform is then applied to produce an absorption spectrum from the interference figure. An interferometer coupled with a microscope allows samples as small as ten micrometers to be analyzed and identified.

2.2.12 Superconducting quantum interference device (SQUID)

A superconducting quantum interference device (SQUID) is a mechanism used to measure extremely weak signals, such as subtle changes in the human body's electromagnetic energy field. Using a device called a Josephson junction, a SQUID can detect a change of energy as much as 100 billion

times weaker than the electromagnetic energy that moves a compass needle. A Josephson junction is made up of two superconductors, separated by an insulating layer so thin that electrons can pass through. A SQUID consists of tiny loops of superconductors employing Josephson junctions to achieve superposition: each electron moves simultaneously in both directions. Because the current is moving in two opposite directions, the electrons have the ability to perform as qubits (that theoretically could be used to enable quantum computing). SQUIDs have been used for a variety of testing purposes that demand extreme sensitivity, including engineering, medical, and geological equipment. Because they measure changes in a magnetic field with such sensitivity, they do not have to come in contact with a system that they are testing. SQUIDs are usually made of either a lead alloy (with 10% gold or indium) and/or niobium, often consisting of the tunnel barrier sandwiched between a base electrode of niobium and the top electrode of lead alloy. A radio frequency (RF) SQUID is made up of one Josephson junction, which is mounted on a superconducting ring. An oscillating current is applied to an external circuit, whose voltage changes as an effect of the interaction between it and the ring. The magnetic flux is then measured. A direct current (DC) SQUID, which is much more sensitive, consists of two Josephson junctions employed in parallel so that electrons tunneling through the junctions demonstrate quantum interference, dependent upon the strength of the magnetic field within a loop. DC SQUIDs demonstrate resistance in response to even tiny variations in a magnetic field, which is the capacity that enables detection of such minute changes.

2.3 Characteristics of undoped GaN

Prior to conduct RE doping, the author optimized the growth conditions of undoped GaN in terms of unintentional electron doping concentration, mobility (μ), FWHM of XRD and the band edge emission peak by exploring on the parameters such as growth temperature, nitridation condition, V/III ratio, and etc. Details are given elsewhere [2-22].

With an optimum growth condition, the unintentional electron doping concentration of 4×10^{17}cm^3 with mobility of 249cm^2/v·s was obtained. FWHM of band edge PL emission and (0002) plane reflection of XRD in ω-2θ mode are 21meV at 77K and ~260 arcsec, respectively.

Fig. 2-14 show TEM images of undoped GaN grown at optimum conditions. The estimated threading dislocation density is ~10^9cm^{-2}. From the selected area diffraction (SAD) pattern (Fig. 2-14 (c)), only the diffraction spots from hexagonal GaN were observed. No secondary phase such as cubic GaN was observed.

P-type conductivity was also obtained by Mg doping. The obtained P-type samples showed hole density range between 8×10^{16}~3×10^{17}cm^{-3} with the mobility between 3~14cm^2/v·s.

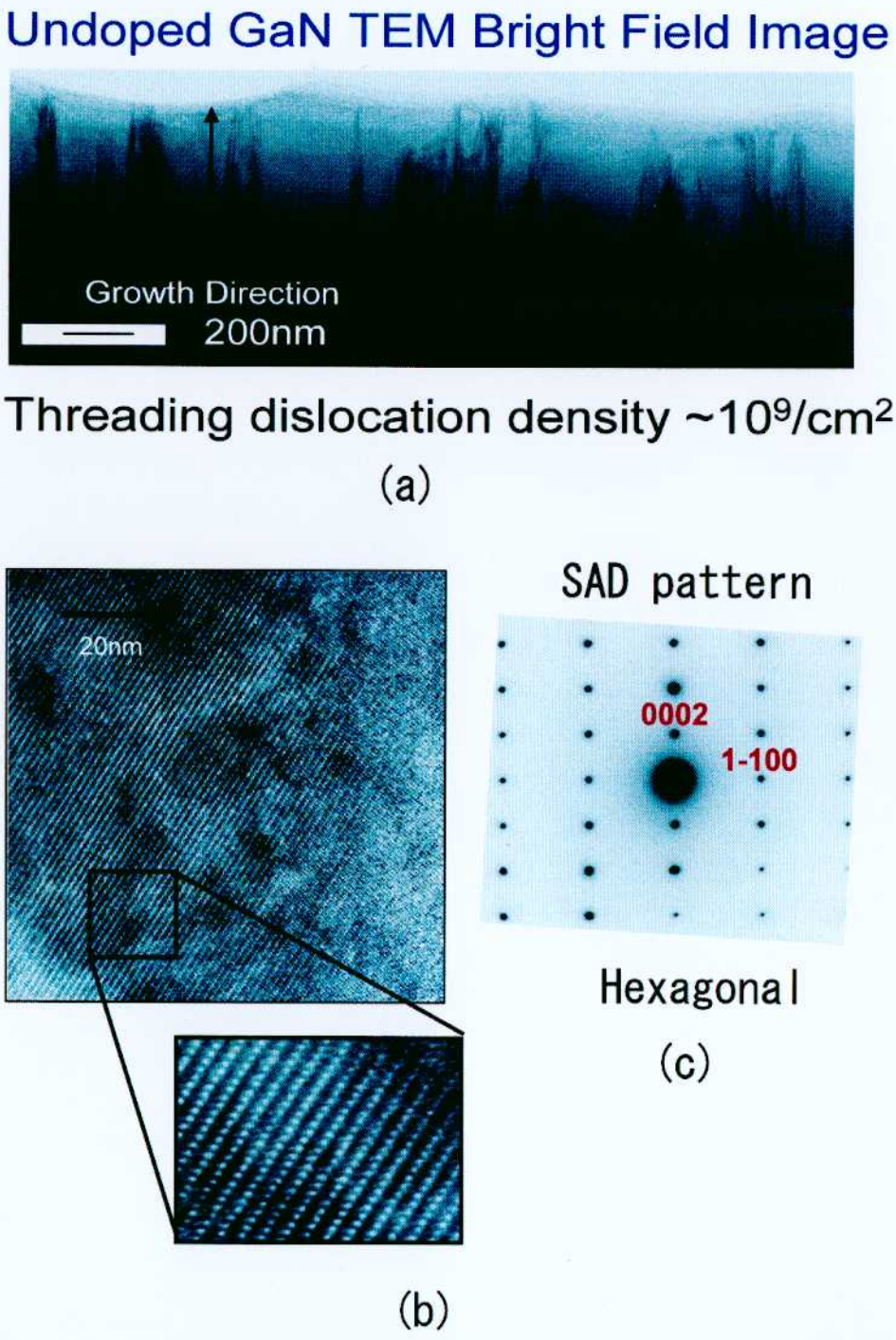

Figure 2-14: (a)A cross sectional TEM image, (b) high resolution TEM image and (c)SAD pattern of undoped GaN grown at optimum conditions.

Chapter 2 References

[2-1] W. Braun, "Applied RHEED", Springer-Verlag (1999).

[2-2] K. Britze and G. Meyer-Ehmsen, Surf. Sci. 77, 131 (1978).

[2-3] K. Inumaru, T. Ohara, S. Yamanaka, Appl. Surf. Sci. 158, 375 (2000).

[2-4] M. Itoh, Phys. Rev. B 58, 6716 (1998).

[2-5] X. Zeng, B. Lin, I. El-Kholy, and H. Elsayed-Ali, Phys. Rev. B 59, 14907 (1999).

[2-6] X. Zeng, B. Lin, I. El-Kholy, and H. Elsayed-Ali, Surf. Sci. 439, 95 (1999).

[2-7] Z. Mitura and J. L. Beeby, J. Phys.: Condens. Matter 8, 8717 (1996).

[2-8] Figures from http://www.hostultra.com/%7Emhegazy/rheed.htm

[2-9] For the review http://www.chembio.uoguelph.ca/educmat/chm729/afm/firstpag.htm

[2-10] Figures from http://stm2.nrl.navy.mil/how-afm/how-afm.html#General%20concept

[2-11] For the review, B. Fultz and J. M. Howe, "Transmission Electron Microscopy and Diffractometry of Materials", Springer New York (2000).

[2-12] B. D. Cullity and S. R. Stock, "Elements of X-Ray Diffraction", Prentice Hall New Jersey (2001).

[2-13] B. E. Warren, "X-Ray Diffraction" Dover, New York (1990).

[2-14] Figures from http://epswww.unm.edu/xrd/xrdbasics.pdf

[2-15] Handbook of Modern Ion Beam Materials Analysis, Editors J. R. Tesmer and M. Nastasi, MRS Pittsburg (1995).

[2-16] T. Maruyama, T. Hasegawa, N. Komuro, H. Yamada, W. Ohtsuka, K. Akimoto, Y. Kitajima, K. Maeda and E. Yagi, J. Appl. Phys. 86 5993 (1999).

[2-17] Boon K. Teo "EXAFS: Basic Principles and Data Analysis", Springer -Verlag (1986).

[2-18] P. A. Lee, P. H. Citrin, P. Eisenberger and B. Kincaid, Rev. Mod. Phys. 53, 769 (1981).

[2-19] D. E. Sayers and B. A. Bunker, X-ray Absorption : "Principles, Applications, Techniques of EXAFS, SEXAFS, and XANES" (Edited by D. C. Koningsberger and R.Prins), Chap. 6. Wiley, Newyork, (1988).

[2-20] A. L. Ankudinov, B. Ravel, J. J. Rehr, and S. D. Conradson, Real Space Multiple Scattering Calculation of XANES, Phys. Rev. B, 7565 (1998).

[2-21] Shinichi Morishima, Hitomi Sasaki, Shunsuke Endo, Takahiro Maruyama, Katsuhiro Akimoto, Yoshinori Kitajima, and Masaharu Nomura, Proceedings of the 2nd International Symposium of Blue Laser and Light Emitting Diodes,242 (1998).

[2-22] Akimoto lab, Group III-V Monthly report, Oct. (2002).